ADVANCING EARTH AND SPACE SCIENCES

Geophysical Research Letters®

RESEARCH LETTER
10.1029/2025GL115811

Lagged Soil Moisture Controls on the Persistence of Drought and Heatwaves in the United States

Kumar P. Tripathy[1], **Ashok K. Mishra**[1], **Sujay V. Kumar**[2], **and Diego G. Miralles**[3]

[1]Zachry Department of Civil & Environmental Engineering, Texas A&M University, College Station, TX, USA, [2]Hydrological Sciences Laboratory, NASA Goddard Space Flight Center, Greenbelt, MD, USA, [3]Laboratory of Hydrology and Water Management, Ghent University, Ghent, Belgium

Key Points:

- Lagged response of surface and rootzone soil moisture (SM) to heatwaves and droughts are quantified using Event Coincidence Analysis
- Rootzone moisture has a stronger and more delayed influence on droughts in the central Plains compared to the Southwest United States
- The prolonged rootzone SM deficit sustained the drought well beyond the occurrence of transient rainfall events

Supporting Information:

Supporting Information may be found in the online version of this article.

Correspondence to:

A. K. Mishra,
ashok_mishra@tamu.edu

Citation:

Tripathy, K. P., Mishra, A. K., Kumar, S. V., & Miralles, D. G. (2025). Lagged soil moisture controls on the persistence of drought and heatwaves in the United States. *Geophysical Research Letters*, *52*, e2025GL115811. https://doi.org/10.1029/2025GL115811

Received 1 APR 2025
Accepted 22 OCT 2025

Author Contributions:

Conceptualization: Kumar P. Tripathy, Ashok K. Mishra
Formal analysis: Kumar P. Tripathy
Funding acquisition: Ashok K. Mishra
Methodology: Kumar P. Tripathy, Ashok K. Mishra
Writing – original draft: Kumar P. Tripathy
Writing – review & editing: Ashok K. Mishra, Sujay V. Kumar, Diego G. Miralles

Abstract Surface soil moisture (SSM) and root-zone soil moisture (RZSM) play critical roles in shaping heatwaves and droughts, yet their distinct controls remain unclear. Using 46 years of North American Land Data Assimilation System Phase 2 data and event coincidence analysis across the contiguous United States, we demonstrate that SSM primarily drives heatwaves in semiarid and sub-humid regions (median MaxTCR ≈ 0.63) through rapid surface drying, which shifts energy from latent to sensible heat. During droughts, RZSM has stronger influence in the central Great Plains (MaxTCR ≈ 0.64–0.71) with 3–5 months lags, indicating prolonged control over transpiration, compared with shorter lags (0–1 month; MaxTCR ≈ 0.44) in the Southwest. Analysis of three major events indicates that RZSM depletion intensified extremes in sub-humid and humid regions by suppressing transpiration and evaporative cooling, whereas sparse vegetation limited these feedbacks in arid regions. Incorporating lagged RZSM data can improve early warning systems for extreme events.

Plain Language Summary This study examines how soil moisture (SM)—both near the surface and deeper in the root zone —influences the development and persistence of droughts and heatwaves across the United States. Analyzing 46 years of weather and soil data, we show that anomalously dry surface soil moisture is closely linked to heatwaves, particularly in semi-arid regions of the central and western United States. Root-zone SM is particularly critical during droughts. In the central Great Plains, for instance, drying in the root zone can initiate or intensify drought conditions, which typically develop three to 5 months after the onset of root-zone drying. Case studies of three major drought and heatwave events show that SM influences these extremes differ by climate regime. In arid regions, SM exerts less control on extreme events due to persistently limited water availability. In contrast, in humid regions, root-zone soil moisture (RZSM) can buffer short dry spells, but once depleted, drought risk increases substantially. Our findings demonstrate that monitoring delayed changes in RZSM could improve early warning systems and help communities better prepare for extreme weather events that threaten water resources, agricultural productivity, and public health.

1. Introduction

Droughts and heatwaves can lead to reduced agricultural productivity (Feng et al., 2019; Zampieri et al., 2017), water scarcity (MacAllister et al., 2020; Mishra & Singh, 2010), socio-ecological impact (Ghanbari et al., 2023) and significant health risks (Mitchell et al., 2016; Mora et al., 2018). Soil moisture (SM) is a key driver in soil-biosphere-atmosphere processes (Green et al., 2017; Liu et al., 2020) and strongly influences the occurrence and severity of droughts and heatwaves (Hirschi et al., 2011; Maraun et al., 2025; Schumacher et al., 2022). Specifically, SM governs the partitioning of surface energy between latent and sensible heat fluxes, which in turn modulates regional weather patterns, including precipitation and temperature (Miralles et al., 2019; Teuling et al., 2013; Zhou et al., 2019). Although SM represents a small fraction of the global freshwater budget, its role in the water cycle and in driving the spatiotemporal evolution of extremes through land–atmosphere interactions is profound (Seneviratne et al., 2010).

Recent studies have shown that surface soil moisture (SSM) anomalies play a critical role in initiating and intensifying droughts and heatwaves, primarily through their impact on land–atmosphere feedbacks and the partitioning of surface energy fluxes (Benson & Dirmeyer, 2023; Guo et al., 2006; Jiang & Wang, 2024; Schumacher et al., 2022). Specifically, reductions in SSM diminish evaporative cooling, resulting in an increase in sensible heat flux at the cost of latent heat flux (Mukherjee et al., 2023; Schwitalla et al., 2025). This change amplifies the soil moisture–temperature (SM–T) feedback, leading to higher surface temperatures. The strength of SM–T feedback differs across climate regions (Mondal et al., 2024; Seneviratne et al., 2010). For instance, in semiarid and subhumid regions (those between arid and humid areas), the feedback is the strongest, as SSM anomalies significantly affect surface fluxes and temperature. The SM–T feedback is weaker in arid regions due to already limited evaporation (Lo et al., 2021), while in humid areas, abundant moisture buffers heat, though prolonged dryness can still reduce cooling and intensify warming (Gevaert et al., 2018; Jiang et al., 2022). Similarly, SSM anomalies play a key role in the onset and persistence of drought through self-propagation. SSM drying in drylands can export water-vapor deficits downwind, extending drought beyond the source region (Schumacher et al., 2022). A Lagrangian analysis of the 40 largest global droughts shows that downwind precipitation falls by about 15% on average (and occasionally by up to 30%) when evaporation diminishes over the desiccated land surface (Schumacher et al., 2022). Additionally, satellite data over the Sahel show that hot, dry soil patches trigger storms that rain on nearby wetter areas, leaving the dry zones drier and reinforcing drought (Barton et al., 2025). The 2010 western Russia event demonstrated that prolonged SM depletion can significantly reduce latent heat flux, sustaining a combined megadrought and heatwave (Miralles et al., 2014).

While SSM has been extensively studied for its role in initiating heatwaves and droughts through land–atmosphere feedbacks, the deeper root-zone soil moisture (RZSM) remains less explored. RZSM contains most of the plant-available water and responds more slowly to climate fluctuations, providing a longer "memory" that can sustain or limit evapotranspiration long after the surface soil has dried (Rahmati et al., 2024; Ruscica et al., 2014). SM memory, or the persistence of anomalies over time, occurs because SM adjusts more slowly than the atmosphere, allowing these anomalies to persist and influence land surface conditions for weeks to months (Koster et al., 2004; Orth & Seneviratne, 2012, 2013). Observational studies across Europe and global drydown analyses demonstrate that while SSM memory dissipates within days to weeks, RZSM memory can persist for months to seasons, particularly in regions with deeper soils, dense vegetation, and moderate aridity (McColl et al., 2017; Orth & Seneviratne, 2013). This extended memory is critical because antecedent RZSM deficits can amplify subsequent heatwaves and droughts by preconditioning the land surface. Beginning the warm season with depleted RZSM reduces latent heat flux, warms the boundary layer, and sustains multi day extreme heat even under identical atmospheric forcing (Miralles et al., 2014). This prolonged influence positions RZSM as a key driver of drought and heatwave persistence; however, its contributions remain poorly quantified due to challenges in large-scale observation and modeling (Rempe & Dietrich, 2018). Although previous studies indicate that RZSM can buffer surface drying and maintain anomalies longer than SSM (Ruscica et al., 2014), comprehensive evaluations of its lagged effects across different climates and ecosystems are still limited.

The above discussion highlights the limited research on the role of RZSM in drought and heatwave events, underscoring the need for a comparative analysis examining both SSM and RZSM across different vegetation types and background aridity levels. Using event-coincidence analysis, we quantify Precursor and Trigger Coincidence metrics to assess the lagged response, direction, and strength of SSM and RZSM impacts on droughts and heatwaves across various climate zones and vegetation types. Such an analysis is essential to quantify the timing, strength, and spatial patterns of SSM and RZSM influence in modulating the severity and persistence of major drought and heatwave events. To achieve this goal, the study investigates (a) how SSM and RZSM anomalies influence the onset and persistence of droughts and heatwaves across the CONUS, and (b) the underlying mechanisms by analyzing three major extreme events, linking SM deficits with changes in surface energy fluxes that drive these extremes. Specifically, it explores how RZSM deficits affect land–atmosphere interactions to intensify or prolong droughts and heatwaves.

2. Data and Methods

2.1. Data

We obtain the 0.125° gridded products from the North American Land Data Assimilation System Phase 2 (NLDAS-2) for the period 1979–2024 across the CONUS (Xia, 2014; Xia et al., 2014). Precipitation data are obtained from a multi-source product combining gauge, radar, and satellite observations (Xia et al., 2012), while the other atmospheric input variables—downward shortwave radiation, downward longwave radiation, 2 m air temperature, 2 m specific humidity, surface pressure, and 10 m zonal and meridional wind components are derived from the 32 km North American Regional Reanalysis (Mesinger et al., 2006) and downscaled to match the NLDAS grid using diurnal interpolation. As part of its multi-model framework, NLDAS-2 provides land-surface outputs from four schemes: Noah-v2.8, Mosaic, SAC, and VIC, all forced with the same atmospheric input data. We select the Noah Land Surface Model (Noah-v2.8) (Noah LSM) because it has demonstrated superior performance when evaluated against observations from the Soil Climate Analysis Network, the United States Climate Reference Network, and AmeriFlux data (Xia, 2014; Xia et al., 2014). Moreover, Noah LSM offers the most accurate representation of both SSM and RZSM variability, exhibiting the lowest mean absolute error (Xia et al., 2015). It also shows no detectable drift over multi-decadal timescales (Xia, 2014; Xia et al., 2014b, 2015; Xia et al., 2015).

To study the influence of SM on heatwaves, hourly atmospheric inputs (e.g., precipitation, $T_{\max}$, $T_{\min}$) are aggregated into daily totals or means to align with the model output frequency of the Noah LSM, which provides daily data for latent and sensible heat fluxes, total evaporation, transpiration, and volumetric SM across four layers (0–10, 10–40, 40–100, and 100–200 cm). All the data sets used in this study are provided in the Table T1 (and Figure S1 in Supporting Information S1). For drought analysis, we use monthly Noah LSM data, including both atmospheric inputs and land-surface outputs. The 0–10 cm soil layer is defined as SSM, while RZSM is derived by calculating the weighted average of three deep layers (10–40 cm, 40–100 cm, and 100–200 cm). Extensive validation studies have shown that the NLDAS-2 ensemble captures the seasonal cycle and interannual variability of SM and reliably reproduces wet and dry events at depths relevant for drought and heatwave analysis (Sun et al., 2018; Xia et al., 2013). Independent satellite-based evaluations further confirm that the Noah model accurately reflects the spatial and temporal patterns of SSM anomalies observed by AMSR-E and produces evapotranspiration estimates that are consistent across CONUS (Tuttle & Salvucci, 2017; Zhang et al., 2020). An overview of NLDAS-2 data, including model development and validation, is provided in Section S1 in Supporting Information S1.

Additionally, we use the MODIS Land Cover Type product (MCD12Q1, Version 6; Friedl et al., 2010) to examine vegetation influences on SM associations with heatwaves and droughts. This data set provides annual global land cover classifications at 500 m resolution, which we reclassify into five dominant vegetation groups (forest, shrubland, grass/savanna, cropland, and urban/barren). To ensure consistency with the NLDAS-2 framework, the MODIS data are aggregated to the 0.125° grid using majority resampling (Section S2 in Supporting Information S1).

2.2. Extraction of Extreme Event Sequences

To examine the relationships between SM and extreme events, the data is converted into binary event series (Figure S2 in Supporting Information S1 and an example in Section S2 in Supporting Information S1). A heatwave is defined as three consecutive days exceeding the 95th percentile of daily maximum temperature for the reference period (1979–2024) (Tripathy & Mishra, 2023). Two heatwaves are treated as distinct if separated by at least 3 days without crossing the threshold. A drought event is defined as when the SPEI falls below the −1.5 threshold and persists for at least 2 months. SPEI-6 is selected for its robustness in capturing both short- and long-term drought conditions, as it integrates precipitation and potential evapotranspiration (PET) over a 6-month scale (Mishra et al., 2015). To ensure the robustness of our findings, we also conducted additional analyses using SPEI-3 (short-term droughts) and SPEI-12 (long-term droughts), demonstrating that the results remain consistent and are not dependent on the specific drought index used. To evaluate the influence of SM on heatwaves, anomalous SSM and RZSM events are defined as periods when values fall below the 5th percentile for at least two consecutive days. For drought analysis, anomalies are identified monthly, requiring SM to remain below the 5th percentile for two consecutive months.

2.3. Event Coincidence Analysis

We employ the ECA method (Donges et al., 2016) to quantify the role of SM at different depths as precursors and triggers for heatwaves and droughts over the CONUS. ECA is a statistical framework that evaluates the strength, directionality, and time lag of interrelationships between pairs of event series (He & Sheffield, 2020; Manoj J et al., 2022; Sun et al., 2018). It provides insights into whether an event in one series precedes (Precursor Coincidence Rate, PCR) or triggers (Trigger Coincidence Rate, TCR) an event in another series.

Let A(t) denote the event series of climate extremes (heat-wave days or drought months) and B(t) denote the event series of soil-moisture deficits (SSM or RZSM dry events). The occurrence times are $t_i^A (i = 1, 2, \ldots, N_A)$ for the extreme events and $t_j^B (j = 1, 2, \ldots, N_B)$ for the soil-moisture events. Both event series are assumed to span the same time interval (t_0, t_f) of length $T = t_f - t_0$ such that $t_0 \leq t_1^A \leq \ldots \leq t_{N_A}^A \leq t_f$ and $t_0 \leq t_1^B \leq \ldots \leq t_{N_B}^B \leq t_f$. Then, PCR can be computed as:

$$\mathrm{PCR}(\tau, \Delta T) = \frac{1}{N_A} \sum_{i=1}^{N_A} H\left(\sum\nolimits_{j=1}^{N_B} I_{[0,\Delta T]}\left(\left(t_i^A - \tau\right) - t_j^B\right)\right) \tag{1}$$

where τ represents the time lag between events in A and B, ΔT is the maximum allowable time window for coincidence, called the time tolerance limit. The Heaviside step function, $H(x) = 1$, if $x > 0$ and 0 otherwise, ensuring only positive contributions and $I_{[0,\Delta T]}(x)$ is the indicator function that ensures coincidence within the specified time window.

PCR evaluates how often an event in series A is preceded by an event in series B. A PCR $= 1$ indicates all events in A are preceded by events in B, while 0 suggests no such precedence. In our context, PCR measures if SM dry events (type-B) are preconditioned with drought or heatwave events (type-A). PCR is a function of the lag parameter τ and the temporal tolerance ΔT. $\tau = 0$ refers to instantaneous coincidence and $\tau \geq 1$ indicates a lagged coincidence.

Similarly, TCR, defined as,

$$\mathrm{TCR}(\tau, \Delta T) = \frac{1}{N_B} \sum_{j=1}^{N_B} H\left(\sum\nolimits_{i=1}^{N_A} I_{[0,\Delta T]}\left(\left(t_i^A - \tau\right) - t_j^B\right)\right) \tag{2}$$

TCR values also range from zero to one, with zero indicating that the extreme SM events (type-B events) have no triggering effects on the type-A event series (dry or hot events).

PCR quantifies whether SM anomalies systematically precede extreme events, indicating a preconditioning role. A high PCR suggests that dry soil conditions are already present before droughts or heatwaves develop, reflecting the influence of antecedent moisture deficits in setting the stage for subsequent extremes. TCR, in contrast, measures whether the occurrence of SM anomalies is followed by extreme events, indicating a triggering or amplifying role. A high TCR indicates that when SM falls below critical thresholds, extreme events are likely to occur after a lag period.

The PCR and TCR values are evaluated for time lags ranging from 0 to 7 days (for hot extremes) and 0–7 months (for dry extremes). Then, we calculated the maximum values of TCR and PCR (MaxTCR and MaxPCR, respectively) along with their corresponding time lags. A detailed calculation procedure for PCR and TCR is provided in Section S2 in Supporting Information S1. Using this information, we calculated $\mathrm{TC}_{\mathrm{ratio}}$ ($\mathrm{PC}_{\mathrm{ratio}}$; see Section S3 in Supporting Information S1) metrics based on the ratio between the maximum TCR (or PCR) values observed during extreme events and their historical baseline values. These ratios provide a relative measure of the enhancement in SM-triggering effects under extreme conditions compared to historical period.

3. Results

3.1. Soil Moisture as a Precursor and Trigger for Heatwave and Drought Events

In the following section, we examine the influence of SM on heatwave and drought extremes across the CONUS. We investigate how lagged SM acts as both a precursor and a trigger for heatwave events on a daily scale and drought events on a monthly scale. Figures 1a and 1b shows the spatial distribution of MaxTCR values for SSM and RZSM, highlighting their influence on heatwave initiation. The MaxTCR metric, described in Section 2.3, measures the strength of the relationship between SM anomalies and their contribution to triggering heatwave events. SSM shows a pronounced influence (MaxTCR $\approx 0.67 \pm 0.14$) concentrated in the central US and parts of the Northwest, consistent with prior findings that surface drying reduces latent heat flux and shifts the energy balance toward sensible heating (Seneviratne et al., 2010; Stéfanon et al., 2014). In contrast, RZSM exerts a stronger influence in the southern and southeastern United States (MaxTCR $>0.6 \pm 0.12$), where deficits in deeper soil layers significantly limit transpiration and reduce evaporative cooling, intensifying and prolonging heatwave conditions (Figure S3 in Supporting Information S1), as also noted by Jiang et al. (2022). A similar assessment is provided by the MaxPCR metric, which indicates the number of heatwaves preceded by SM

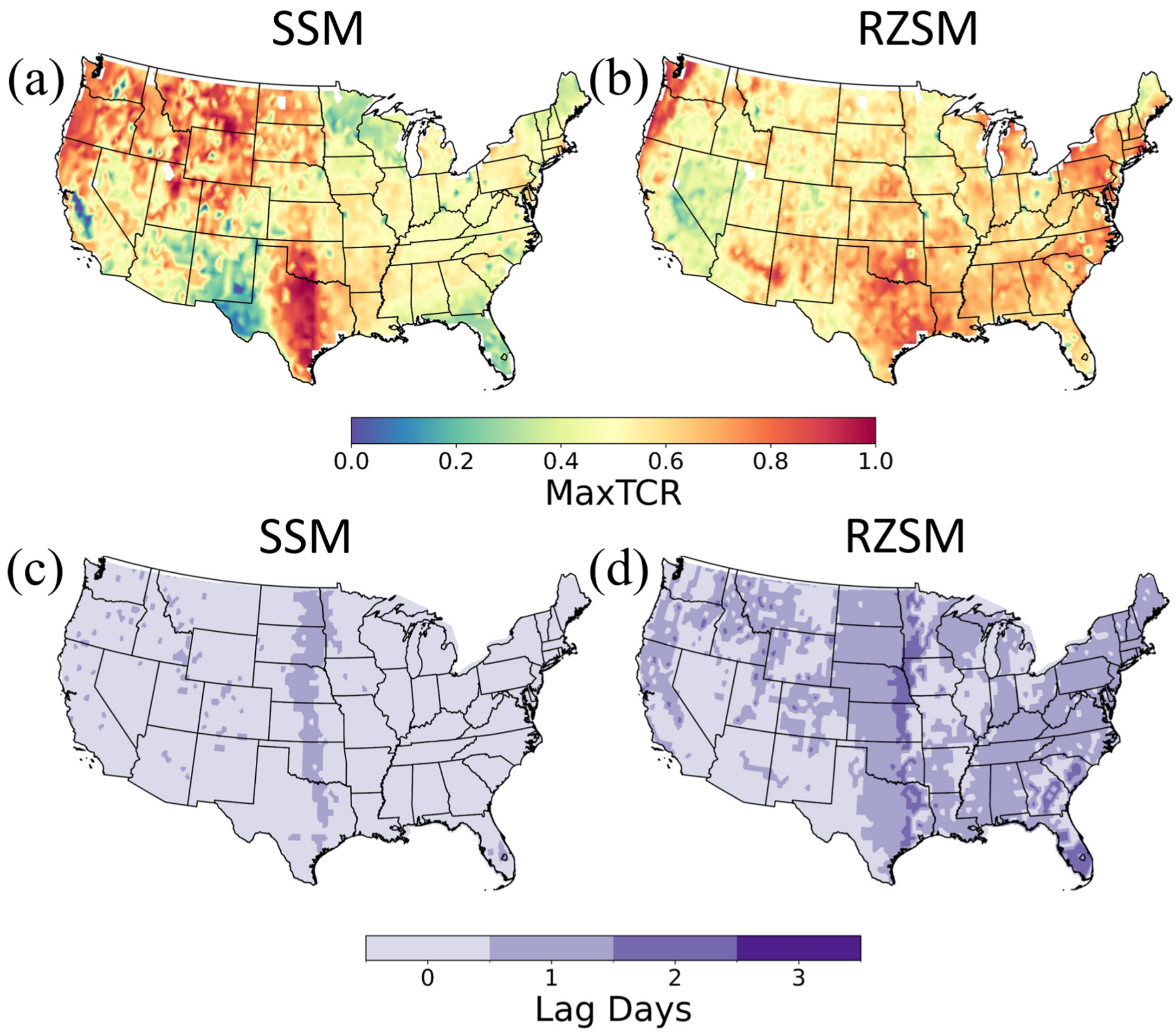

Figure 1. Surface and rootzone soil moisture (SM) as a Precursor and Trigger for Heatwave Events: Spatial maps (a)–(b) show MaxTCR distribution for (a) surface and (b) root zone soil layers, highlighting spatial variability in SM's role in triggering heatwaves. Panels (c)–(d) depict lag times (0–3 days) for surface and root zone layers, indicating the delay between SM anomalies and heatwave onset.

anomalies; the corresponding results are presented in Figure S4 in Supporting Information S1. Conversely, heatwave events in the northwestern and central United States exhibit weak associations with RZSM anomalies, likely reflecting regional differences in climate, vegetation, and soil properties that affect moisture availability and land–atmosphere interactions (Benson & Dirmeyer, 2021). In arid regions, persistently low water availability weakens SM–temperature feedbacks, whereas in humid areas, dense vegetation and greater soil water-holding capacity help buffer RZSM depletion. Additionally, sparse vegetation in arid zones limits transpiration regardless of RZSM conditions, thereby reducing the influence of RZSM on heatwave development. These regional controls on SM–extreme relationships are quantified in detail in Section 3.3.

Figures 1c and 1d shows the corresponding lag times associated with the MaxTCR values, indicating the delay between SM anomalies and the onset of heatwave events. SSM exhibits rapid influence with near-zero lag across the eastern and western US, consistent with shallow layers responding quickly to radiative forcing. However, in the central and Great Plains regions, SSM lag times increase to ∼1–2 days, indicating a delayed yet intensified interaction between SM deficits and atmospheric heating. RZSM exhibits longer lag times, up to 3 days, particularly in the Great Plains, where infrequent precipitation limits deep soil recharge and moisture in deeper

10.1029/2025GL115811

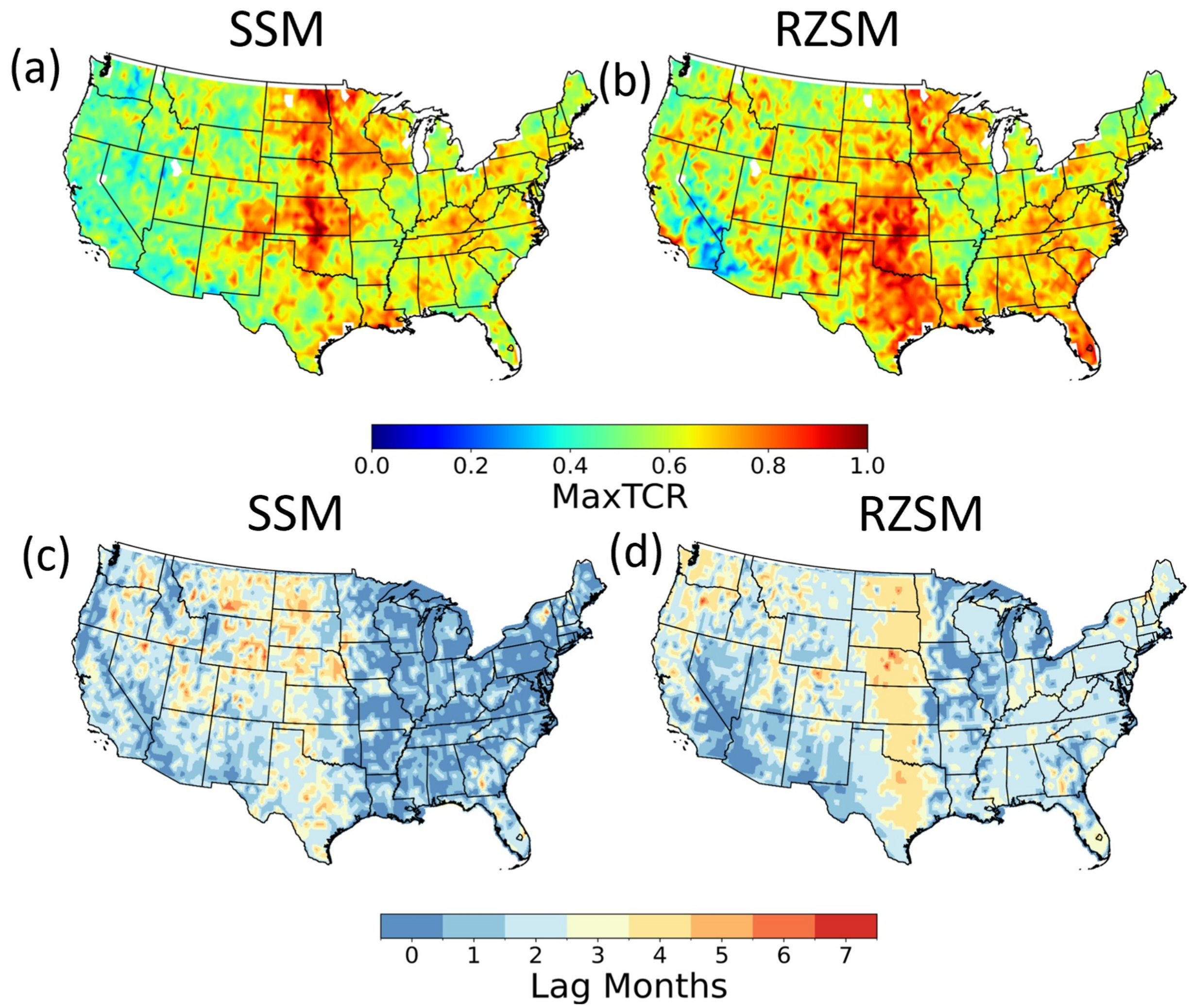

Figure 2. Surface and rootzone soil moisture (SM) as a Precursor and Trigger for Drought Events: Spatial maps (a)–(b) show MaxTCR distribution for (a) surface and (b) root zone soil layers, highlighting spatial variability in SM's role in triggering drought events. Panels (c)–(d) depict associated lag times (0–7 months) for surface and root zone layers, indicating the time lag between SM anomalies and the onset of drought conditions.

layers responds more slowly to atmospheric demand (Ford et al., 2015). In arid regions of the Southwest US, US lag times are near zero (even for RZSM) primarily due to limited SM availability and rapid evaporation, which inhibit retention and storage in rootzone layers (Hao et al., 2024; Koster et al., 2004). These regions receive sparse and infrequent rainfall, offering minimal opportunity to recharge RZSM. As a result, during a heatwave, the lack of deep moisture reserves leads to rapid soil heating, which elevates near-surface temperatures and intensifies the severity of the event. In the absence of the buffering effect provided by RZSM, heat transfer from subsurface layers to the surface becomes more efficient, further enhancing surface warming and exacerbating heatwave conditions. In contrast, in the more humid eastern regions, RZSM anomalies typically lag heatwave peaks by about one day, indicating a more immediate role in moderating heatwaves through evaporative cooling (Dirmeyer et al., 2021).

We analyzed the influence of SSM and RZSM on drought extremes across the CONUS, using the 6-month SPEI (SPEI-6) as the primary metric. This medium timescale was chosen for its ability to capture seasonal variability while balancing the sensitivity to both short-term (e.g., 3-month) and long-term (e.g., 12-month) drought conditions. SSM in the central Great Plains exhibits the highest MaxTCR values (0.72 ± 0.12; Figure 2a), indicating a strong association between SM deficits and drought onset. This reflects the region's sensitivity to land–atmosphere feedbacks, where SM anomalies play a key role in influencing energy flux partitioning and atmospheric processes (Gevaert et al., 2018). In contrast, the southwestern US exhibits significantly lower MaxTCR

10.1029/2025GL115811

values (∼0.39 ± 0.07), largely due to limited precipitation and high potential evaporation, which reduce the influence of SM. When considering RZSM, its role in drought initiation becomes more prominent, showing a stronger association with SPEI, as reflected by higher MaxTCR values compared to SSM (Figure 2b). This enhanced impact of RZSM on drought onset is particularly evident across the Great Plains, central states, and the humid East and Southeast, underscoring its critical role in sustaining drought conditions. RZSM deficits prolong drought by limiting water availability, increasing evaporative losses, disrupting regional water cycles (e.g., lowering humidity), and suppressing precipitation, ultimately slowing recovery and extending drought duration (Hirschi et al., 2014) A similar pattern emerges in the MaxPCR results, where RZSM anomalies more consistently precede drought onset compared to SSM across most regions (see Figure S7 in Supporting Information S1). To ensure the robustness of these findings across different timescales, additional analyses using SPEI-3 and SPEI-12 were performed, yielding consistent results (Figures S5–S6 in Supporting Information S1).

Figures 2c and 2d presents the corresponding lag times associated with the maximum TCR values, which vary regionally. In the surface layer, the shortest lag times (approximately 0–1 month) are observed in the humid Eastern US, where frequent precipitation enables rapid SM recharge and facilitates quicker recovery (Ford & Labosier, 2017). Similarly, the Southwest shows near-zero lag times, primarily due to rapid evaporation and limited SM availability (Li et al., 2024). In contrast, the semi-arid to sub-humid Great Plains exhibit longer lag times of 1–4 months, reflecting a combination of moderate precipitation and soils with high water-holding capacity that enable the root zone to buffer against dry periods (Li et al., 2024).

Lag times increase further for RZSM, reaching 2–4 months across the Great Plains and western US, and ranging from 1 to 3 months in the East. These regional differences are influenced by soil texture and moisture dynamics. In the East, sandy soil promotes rapid infiltration but also quick drying, resulting in moderate lag times. In contrast, the clay- and silt-rich soils of the Great Plains slow moisture recharge, leading to longer lag responses (Ford & Labosier, 2017). In the Southwest, root-zone lag times remain short (∼1 month) due to high evaporative demand and limited moisture retention, which restricts the soil's capacity to function as a reservoir. Collectively, variations in soil characteristics, vegetation, and climate across regions play a critical role in shaping the timing and persistence of drought conditions across the CONUS.

3.2. Soil Moisture Influence on Heatwaves and Droughts: Three US Case Studies

3.2.1. SM Influence on Heatwave

To examine how SSM and RZSM influence heatwave development and persistence, we analyze three major events across distinct hydroclimatic regions: the 2007 southeast heatwave, the 2012 Midwest heatwave, and the 2021 southwestern heatwave (refer Section S5 in Supporting Information S1 for the selection of these extreme events). These events were chosen because they rank among the most significant in terms of severity, spatial coverage and duration, thereby providing representative case studies across diverse climate regimes. Among the 66 major heatwave events identified during 1979–2024 (Table S5.2 in Supporting Information S1), the 2007 Southeast event exhibits the highest average severity (32.9°C), while the 2012 Midwest event ranks first in spatial extent (79.2% of CONUS) and second in severity (31.6°C). The 2021 Southwest event ranks fourth in severity (27.1°C) and occurred during a multi-year megadrought. We discuss the 2007 southeast event in detail to illustrate key land–atmosphere processes (Figure 3), while detailed diagnostics for the other two events are provided in Figures S8 and S9 in Supporting Information S1. In late summer 2007, the southeastern US experienced a brief but intense heatwave (Goodrich et al., 2011), with daily mean air temperature anomalies exceeding +1.5°C for much of the period from July 29 to August 19, reaching a maximum of +1.9°C on August 13 (Figure 3a). The rise in temperature was compounded by intermittent rainfall (1–3 mm d^{-1}), which temporarily increased SSM; however, RZSM continued to decline, falling below -2.5σ (where σ denotes the standard deviation) by early August (Figure 3b). Initially, transpiration rate increased in response to elevated evaporative demand under rising air temperatures; however, as the heatwave progressed and RZSM dropped below the vegetation stress threshold, transpiration sharply declined from approximately 4 mm d^{-1} to 2 mm d^{-1} (Figure 3c). Meanwhile, soil evaporation remained minimal throughout the event (<0.5 mm d^{-1}). As moisture depletion continued, canopy conductance declined due to stomatal closure, resulting in a breakdown of plant-mediated cooling. This shift is evident in the surface energy budget: the Bowen ratio (Figure 3c), which represents the partitioning of net radiation between sensible and latent heat fluxes, rose from 0.31 at the onset of the heatwave to 0.57 at its peak—indicating a clear transition from evaporative cooling to sensible heating.

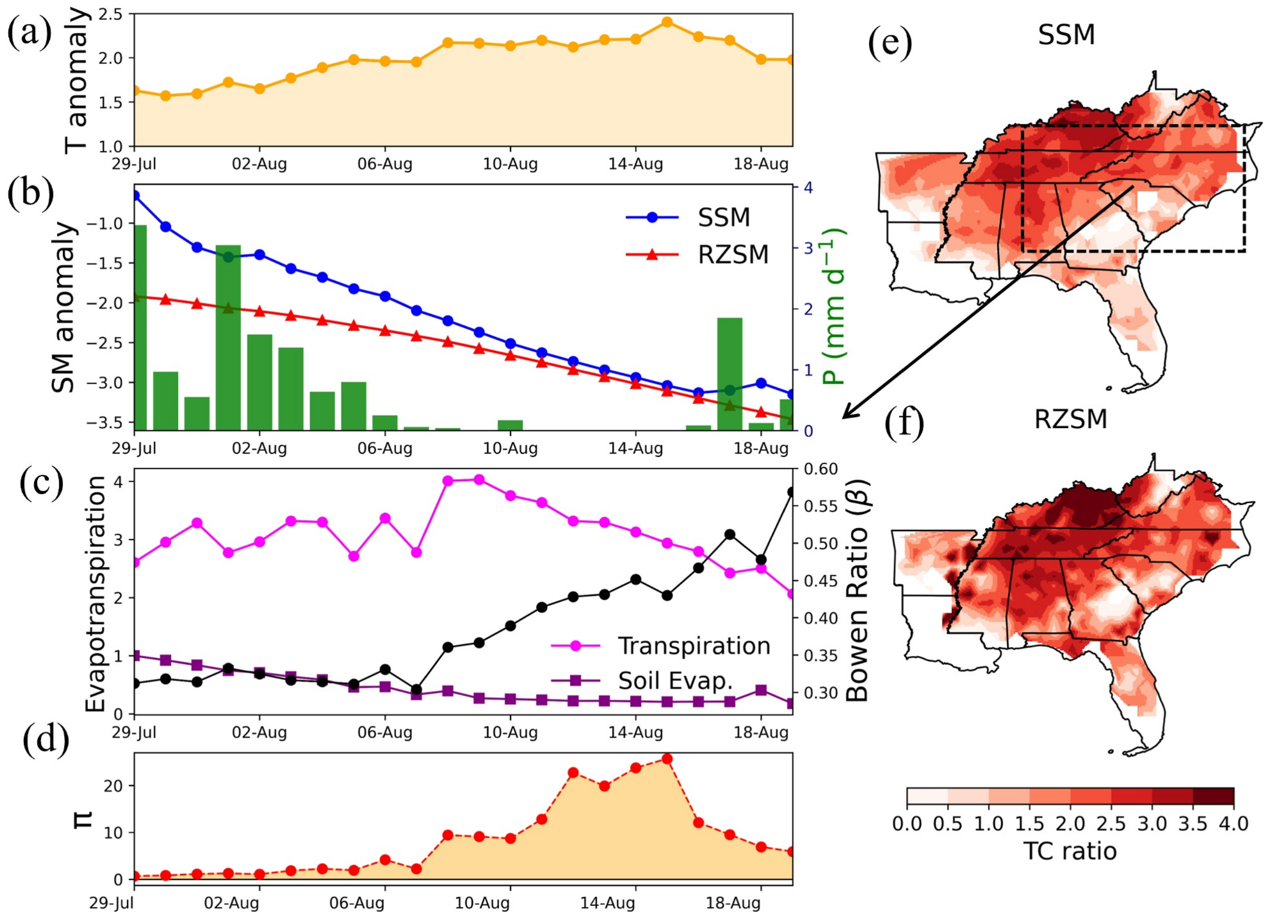

Figure 3. Figure illustrates the role of SSM and root-zone soil moisture (RZSM) anomalies in the evolution of the 2007 Southeast USA heatwave. Panel (a) shows the time series of temperature anomaly, while panel (b) presents soil moisture anomalies for both SSM and RZSM. Panel (c) displays the daily time series of transpiration, soil evaporation, and the Bowen ratio (right y-axis). The soil moisture–temperature coupling metric plotted on a daily scale is shown in panel (d). Finally, panels (e) and (f) compare the TC ratios for SSM and RZSM over Southeast USA, respectively.

The short-term soil moisture–temperature (SM–T) coupling metric (π; see Section S6 in Supporting Information S1 for calculation details (Miralles et al., 2012),) was initially 1.6 during the period of rising transpiration. As the heatwave progressed, π steadily increased, eventually exceeding 20, indicating a strong intensification of SM–T feedback that amplified the severity of the event (Figure 3d). This transition was predominantly controlled by the availability of RZSM. During the 22-day heatwave, transpiration showed a strong and statistically significant correlation with RZSM ($r = 0.48$, $p < 0.01$), whereas its correlation with SSM was weak and not statistically significant ($r = 0.21$, $p = 0.34$). As the event progressed and RZSM declined, total evaporative cooling—which includes plant transpiration, bare-soil evaporation, and canopy interception loss—decreased by more than 50%. Among these components, transpiration was the dominant contributor to latent heat flux and was directly sustained by RZSM availability (Figure S10 in Supporting Information S1). Once RZSM dropped below the vegetation stress threshold, transpiration sharply declined, along with the minor contributions from soil and canopy evaporation. This reduction in total latent heat flux shifted the surface energy balance toward increased sensible heating, causing more energy to accumulate in the boundary layer, thereby reinforcing near-surface warming and amplifying land–atmosphere coupling. Furthermore, the TCratio—which compares the event-specific MaxTCR to its historical baseline MaxTCR (see Section S3 in Supporting Information S1)—was significantly higher for RZSM (~4.0) than for SSM (~2.5), highlighting the dominant role of RZSM in controlling heatwave persistence (Figures 3e and 3f).

During the 2012 Midwest heatwave, much like the 2007 event in the Southeast, SSM and RZSM started below normal (~−1σ) and dropped further to ~ −2.5σ as temperatures peaked. Initially, transpiration rose to 5 mm d^{-1},

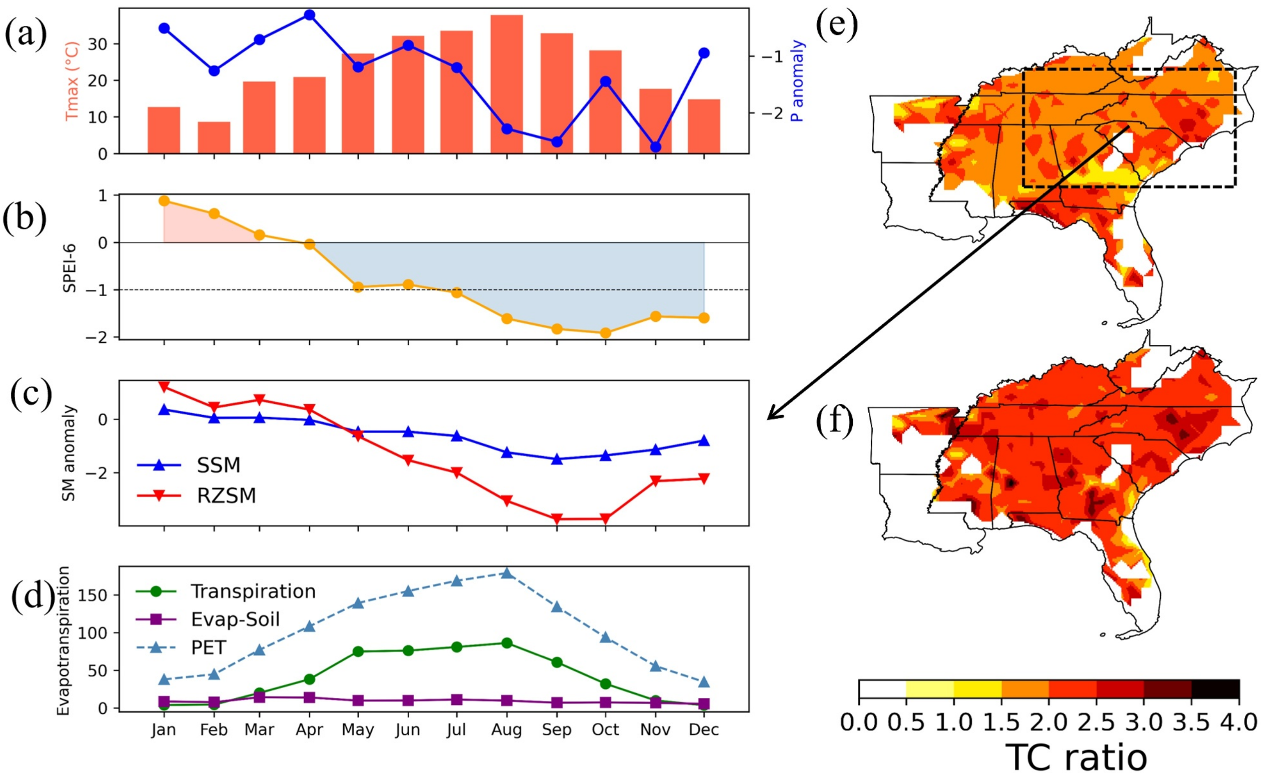

Figure 4. The figure illustrates the role of monthly surface soil moisture (SSM) and root zone soil moisture (RZSM) anomalies in the evolution of the 2007 Southeast U. S. drought. Panel (a) shows the time series of spatially averaged monthly temperature (°C, bars) and monthly precipitation anomalies (right *y*-axis); (b) displays the monthly SPEI-6 time series; (c) shows the monthly anomalies of SSM and RZSM; (d) illustrates monthly time series of potential evapotranspiration (PET, dotted blue), transpiration (green), and bare-soil evaporation (purple). Finally, panels (e) and (f) compare the TCratio for SSM and RZSM over Southeast USA for the year 2007.

but as the heatwave continued, reduced plant water uptake caused transpiration to steadily drop to ~2 mm d^{-1} (Figure S8 in Supporting Information S1). With minimal bare soil evaporation, reduced plant water uptake sharply lowered latent heat flux, diverting more net radiation to sensible heat. This shift increased π above 10, indicating stronger land-atmosphere feedbacks that prolonged the heatwave.

In contrast, during the 2021 heatwave over the Southwest, rainfall was nearly absent (<0.1 mm d^{-1}), and both SSM and RZSM anomalies were already negative, drier than the initial conditions in the Midwest or Southeast. Due to the barren land dominated, bare soil evaporation dominated transpiration, starting at approximately 1 mm d^{-1} before dropping to about 0.1 mm d^{-1} as the surface dried (Figure S9 in Supporting Information S1). Sparse vegetation kept transpiration inherently low, declining only from 0.54 to 0.40 mm d^{-1}, a much smaller reduction compared to those observed in the Midwest and Southeast heatwaves in subhumid to humid regions. Consequently, the π rose only to ~3, indicating a significantly weaker SM influence on temperature compared to the prior two heatwaves. Together, these three heatwave case studies demonstrate that root zone soil drying amplifies and prolongs heatwaves in subhumid to humid regions by suppressing plant evaporative cooling, whereas low transpiration limits feedback strength in arid regions.

3.2.2. SM Influence on Drought

We investigated the drought event that coincided with the 2007 Southeast US heatwave, which developed in three distinct stages. From January to April, drought conditions remained within the normal range (SPEI-6 > 0), with regional average precipitation anomalies ~ -0.3σ compared to the 1979–2024 mean (Figure 4a). Despite this moderate shortfall, RZSM anomalies remained positive, supporting near-normal transpiration rates. However, in May, drought conditions intensified significantly as precipitation dropped to nearly 50% of the long-term average, while PET exceeded 150 mm $month^{-1}$. This sharp increase in atmospheric moisture demand led to a rapid decline in SPEI-6 values, which fell from positive territory in April to −1 by May (Figure 4b). SSM responded quickly, exhibiting negative anomalies by early May, while RZSM began to show signs of depletion, though it remained less impacted than SSM at this stage (Figure 4c). The drought that began in May persisted from June through August, as ongoing precipitation deficits combined with elevated PET intensified atmospheric moisture demand. This led to continued soil drying, which gradually extended downward into the root zone. By June, SSM anomalies had declined to around -0.5σ, while RZSM anomalies dropped more sharply to -1.0σ, indicating deeper and more persistent drying. By August, regional-mean RZSM anomalies reached a critical low of approximately -2.6σ, signaling severe SM depletion, whereas SSM anomalies stabilized near -0.9σ (Figure 4c). This divergence highlights the greater severity and slower recovery of RZSM compared to SSM under prolonged hydrometeorological stress, consistent with its longer memory in humid regions (Jiang et al., 2022).

The decline in RZSM limited plant water uptake and induced stomatal closure, leading to a steady reduction in transpiration—from ~67 mm month^{-1} in August to ~30 mm month^{-1} by October (Figure 4c). With bare-soil evaporation and canopy interception already minimal, total latent heat flux dropped significantly. This reduction in evaporative cooling shifted the surface energy balance toward increased sensible heat flux, promoting boundary-layer warming and inhibiting convective precipitation, thereby intensifying the drought. These land–atmosphere feedbacks are evident in the TCratios across Alabama, Georgia, and the Carolinas. The RZSM anomalies exhibited a 3–4-fold increase in co-occurrence with SPEI-6 drought conditions, while SSM anomalies showed a more modest 1.5–2-fold enhancement (Figures 4e and 4f).

The persistence of the RZSM deficit, attributable to its long residence time, allowed the drought to persist well beyond transient rainfall events. For instance, despite an October rainfall event of ~80 mm, the RZSM anomaly remained near -3σ and the SPEI-6 index stayed below -1.5 for several weeks, demonstrating that even substantial precipitation cannot rapidly restore RZSM (Figure 4c). This sequence of winter precipitation shortfall, progressive RZSM depletion, reduced transpiration, and diminished latent cooling illustrates a self-reinforcing pathway by which RZSM governs both the intensity and longevity of drought.

Comparable diagnostics for the 2012 Midwest drought and the 2021 southwestern USA megadrought (Figure S11 in Supporting Information S1) reveal that this mechanism operates across diverse hydroclimatic regimes, further emphasizing the widespread role of RZSM in drought evolution. However, in arid ecosystems such as the southwestern USA during the 2021 drought (Figure S12 in Supporting Information S1), where vegetation cover is sparse and transpiration rates are low, the influence of RZSM on drought development is comparatively weaker. In such regions, where shrublands and barren lands dominate, atmospheric control and surface processes may play a more dominant role.

3.3. Aridity and Vegetation Effects on Soil Moisture Influence Over Extremes

3.3.1. Influence of Background Aridity

Spatiotemporal patterns of precipitation and evapotranspiration play a key role in the development of droughts and heatwaves, with SM dynamics further modulated by background aridity (Mukherjee & Mishra, 2021). To examine the influence of background aridity, we divide the CONUS into four climate regions based on the Aridity Index (AI): arid ($AI < 0.2$), semi-arid ($0.2 \leq AI < 0.5$), sub-humid ($0.5 \leq AI < 0.65$), and humid ($AI \geq 0.65$). The AI is calculated as the ratio of mean annual precipitation to PET over the period 1979–2016 (Mukherjee & Mishra, 2021) (Figure 5a).

Our findings reveal a clear spatial gradient in heatwave sensitivity to SM, with the strongest SSM–heatwave associations (median MaxTCR $\approx$ 0.63) observed in semi-arid and sub-humid regions (Figure 5b) (Lorenz et al., 2010; Mueller & Seneviratne, 2012). These transitional climates offer both sufficient water and energy, allowing even small SSM anomalies to significantly alter the surface energy balance from latent to sensible heat flux. In arid regions, the association is comparatively weaker (median MaxTCR $\approx$ 0.51) due to persistently low SM, which limits evaporation and weakens land–atmosphere feedbacks. Humid regions exhibit the weakest response (median MaxTCR $\approx$ 0.48), as abundant moisture buffers temperature increases and dampens heatwave amplification. RZSM also influences heatwaves in semi-arid and sub-humid regions (median MaxTCR $\approx$ 0.52), albeit with a delayed effect due to the deeper location of moisture reserves. Notably, in humid regions, RZSM shows slightly stronger control than SSM (median MaxTCR $\approx$ 0.51), likely because it helps sustain transpiration when surface soils remain moist but root-zone moisture begins to decline (Lorenz et al., 2010; Mueller & Seneviratne, 2012).

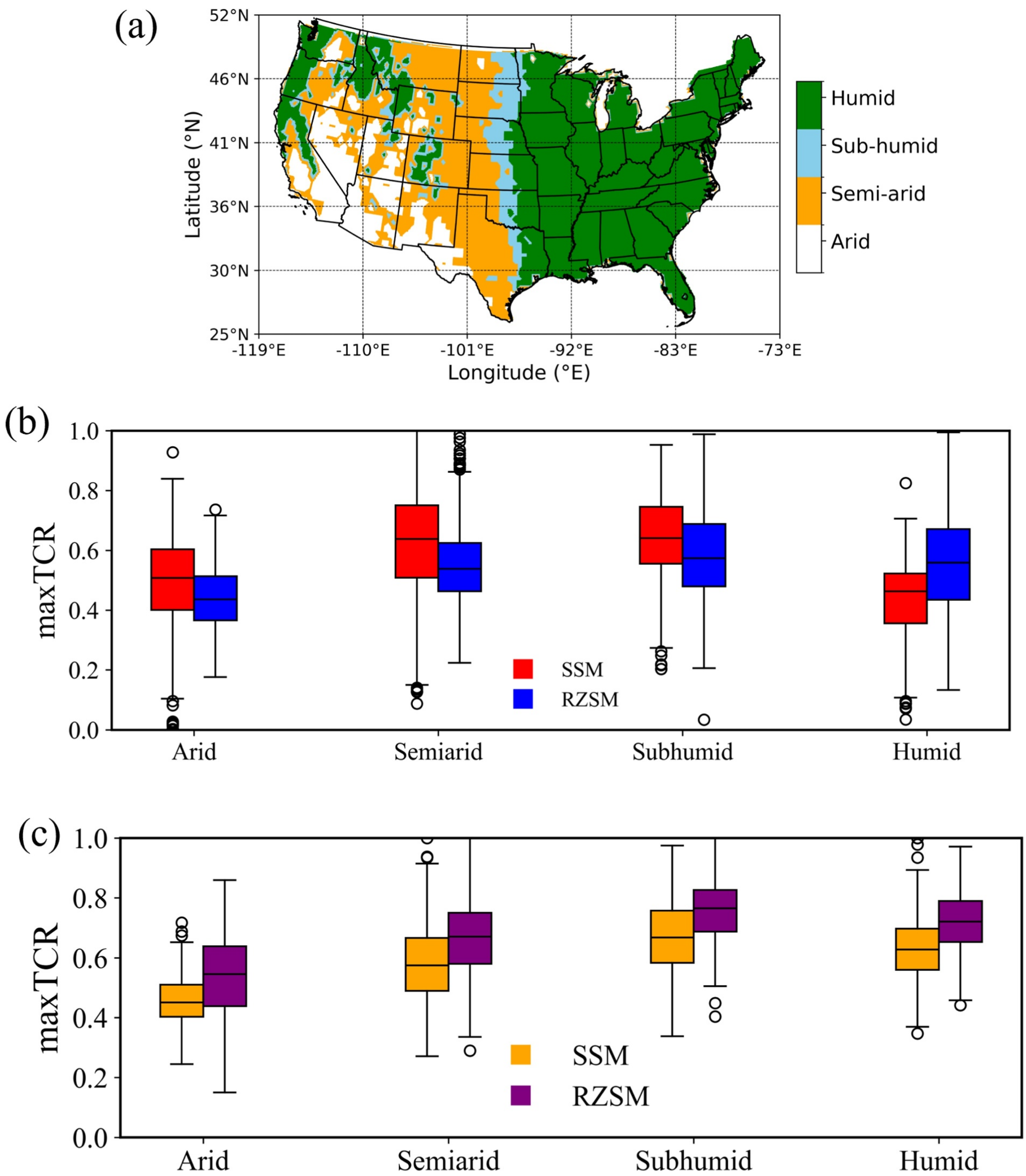

Figure 5. Effects of background aridity on soil moisture control of drought and heatwaves. (a) Aridity-Index map of the CONUS, showing four climate zones: Arid ($AI < 0.20$), Semi-arid ($0.20 \le AI < 0.50$), Sub-humid ($0.50 \le AI < 0.65$), and Humid ($AI \ge 0.65$). (b) Box-and-whisker plots showing MaxTCR values for heatwave events, comparing SSM and root-zone soil moisture (RZSM) across the four aridity classes. (c) Box-and-whisker plots of MaxTCR values for drought events, comparing SSM and RZSM across the same aridity classes.

For drought initiation and persistence (Figure 5c), SSM has comparatively less influence in arid regions (median MaxTCR ≈ 0.44) due to rapid depletion of shallow moisture, but its impact increases in semi-arid areas (median MaxTCR ≈ 0.51). This influence becomes even stronger in sub-humid (MaxTCR ≈ 0.61) and humid zones (MaxTCR ≈ 0.56), where higher precipitation enables SSM anomalies to more effectively modulate short-term drought onset. In contrast, RZSM exerts its greatest, though delayed, impact in sub-humid (median

MaxTCR ≈ 0.71) and semi-arid regions (MaxTCR ≈ 0.64), reflecting its longer retention time and capacity to sustain evapotranspiration and land–atmosphere feedbacks (Orth & Seneviratne, 2012). Even in humid climates, RZSM deficits can prolong drought by limiting plant transpiration and maintaining low latent heat fluxes, thereby intensifying and extending drought risks (Cammalleri et al., 2024; Ji et al., 2021; Tijdeman & Menzel, 2021).

3.3.2. Influence of Vegetation Types

To quantify how SM control on heatwaves and droughts varies across vegetation types, we utilize MODIS land cover data (MCD12Q1) and reclassify the original 17 land cover classes into five dominant categories: Forest, Shrubland, Grass/Savanna, Cropland, and Urban/Barren (Figure S8.1a–b in Supporting Information S1). For heatwaves, croplands exhibit a stronger influence from SSM (Figure S8.1c in Supporting Information S1; median MaxTCR = 0.68), likely due to their shallow rooting systems and sparse canopy cover, which promote rapid surface drying under high temperatures (Vasconcelos & Sacht, 2020). Grasslands exhibit slightly lower but still considerable SM influence, with median MaxTCR values of ∼0.62 for SSM and ∼0.58 for RZSM. Similarly, urban and barren areas demonstrate strong control by the surface layer, with median MaxTCR values ∼0.60 for SSM and ∼0.57 for RZSM. In contrast, forested regions respond more to RZSM (∼0.59), reflecting their deeper roots (2–3 m rooting depth; Zeng, 2001) and larger canopy water storage, while their surface-layer influence is slightly lower (∼0.55).

During drought conditions, RZSM exerts a stronger influence across all vegetation types, underscoring the critical role of subsurface moisture in sustaining prolonged droughts. Croplands remain the most sensitive to RZSM (median MaxTCR ∼0.75), reflecting their dependence on shallow SM because of limited root depth and minimal canopy protection. Grasslands and shrublands show moderate control by RZSM (∼0.59 and ∼0.57, respectively), both exceeding the influence of SSM. Forests also respond more to RZSM (∼0.56) than to SSM (∼0.52), while urban and barren areas exhibit the smallest difference between the two layers, likely due to low SM availability and retention capacity. A detailed discussion of these findings can be found in Section S8 in Supporting Information S1.

4. Discussion and Conclusion

Droughts and heatwaves increasingly threaten ecosystems and societies by disrupting water supplies, agriculture, and health. These extremes are closely linked to SM anomalies, where low SM intensifies sensible heat and surface temperatures through land-atmosphere feedbacks (Jiang & Wang, 2024; Miralles et al., 2014; Schumacher et al., 2022). This study uses ECA to quantify SM's role in droughts and heatwaves across surface and root-zone layers by assessing the strength and timing of their relationships. Results show that SSM deficits quickly trigger heatwaves, especially in semi-arid and sub-humid regions (median MaxTCR ≈ 0.63), while RZSM anomalies respond more slowly but sustain reduced transpiration, prolonging warming.

Background aridity critically influences SM interactions with climate extremes. Semi-arid to sub humid regions exhibit the greatest heatwave sensitivity to both SSM and RZSM anomalies, reflecting a balance between water availability and atmospheric demand (Mueller & Seneviratne, 2012). In contrast, arid areas display weak SM and extreme event links and near zero lag times due to limited moisture and high evaporation. While humid regions can buffer short term SSM deficits, prolonged drought occurs when RZSM is depleted, with lag times of 2–4 months. The central Great Plains experience the longest RZSM lag times—3 to 5 months—highlighting delayed SM responses in drought development. Vegetation influences SM's impact on climate extremes. Croplands show strong heatwave sensitivity to SSM due to shallow roots (<1 m rooting depth), while forests respond more to RZSM because of deeper roots (2–3 m rooting depth; Zeng, 2001) and canopy storage. For droughts, RZSM consistently has a stronger role across vegetation types, highlighting its importance in sustaining prolonged dry spells.

Our analysis shows that RZSM significantly sustains and amplifies drought–heatwave events, especially in sub-humid and humid regions. Our case study findings build upon and complement previous research on these well-documented extreme events. The 2007 Southeast drought-heatwave has been extensively analyzed by Seager et al. (2009), who attributed it primarily to precipitation deficits driven by atmospheric circulation anomalies and weak La Niña influence, with evaporation declining alongside precipitation. Our results confirm that precipitation deficits initiated the event but reveals a critical amplification mechanism that was not previously quantified. During the 2007 Southeast US heatwave, RZSM declined sharply despite short-term rainfall replenishing SSM, reducing transpiration from ∼4 to 2 mm d^{-1} and latent heat. This weakened evaporative cooling increased sensible heating, deepening the boundary layer and reinforcing surface warming. The SM–T coupling (π) and TCratio were higher for RZSM (∼4.0) than SSM (∼2.5). Transpiration exhibited strong correlation with RZSM ($r = 0.48$, $p < 0.01$) but not SSM ($r = 0.21$, $p = 0.34$), demonstrating that land-surface feedbacks operated through RZSM depletion to sustain both the heatwave and drought conditions—an amplification pathway not previously quantified. In contrast, the 2021 Southwestern event showed weaker feedbacks due to sparse vegetation and low transpiration. Williams et al. (2022) documented this event as the driest 22-year period since at least 800 CE, attributing it primarily to precipitation deficits and elevated temperatures amplified by anthropogenic warming. Our finding that SM-temperature coupling remained weak (π ∼3) despite severe drought conditions confirms that in water-limited ecosystems with sparse vegetation, atmospheric forcing dominates over land-surface feedbacks—consistent with modeling studies showing limited SM–T coupling in arid regions (Gevaert et al., 2018; Seneviratne et al., 2010). Collectively, while previous studies identified atmospheric drivers of drought initiation, our analysis demonstrates that RZSM depletion represents a critical amplification mechanism that sustains and intensifies heatwaves and droughts in sub-humid to humid regions through suppressed transpiration (Fu et al., 2024)—a process that is weak in vegetation-sparse arid regions.

One limitation of our study is the challenge of separating SSM and RZSM effects, as these layers are often correlated (Hirschi et al., 2014). Additionally, droughts and heatwaves result from complex interactions among atmospheric circulation patterns, oceanic teleconnections, and land-atmosphere feedbacks (Di Lorenzo & Mantua, 2016; Lemus-Canovas et al., 2024; Miralles et al., 2014; Wang et al., 2025). While the Event Coincidence Analysis used in this study captures links between SM anomalies and extreme events, it cannot isolate SM effects from larger-scale drivers (Donges et al., 2016). To address these limitations, controlled numerical experiments are needed that: (a) selectively fix or alter SM in specific layers within coupled land surface models to disentangle SSM versus RZSM contributions, and (b) use atmosphere-only simulations with prescribed versus interactive SM to separate land-atmosphere feedbacks from large-scale atmospheric forcing (Seneviratne et al., 2006). Furthermore, Future research should explore how vertically uniform versus heterogeneous SM profiles (with the same total moisture) affect evaporation, heat partitioning, and near-surface temperature responses. This study highlights the importance of accurately representing RZSM in monitoring and forecasting systems to improve early warnings for heatwaves and droughts. Enhancing land-surface models with depth-dependent SM processes will improve seasonal climate predictions and aid adaptation efforts to safeguard food security, water resources, and ecosystem health amid climate warming.

Conflict of Interest

The authors declare no conflicts of interest relevant to this study.

Data Availability Statement

North American Land Data Assimilation System Phase 2 Noah Land Surface Model data (1979–2024) including precipitation, temperature, SM (four layers: 0–10, 10–40, 40–100, 100–200 cm), evapotranspiration, and surface energy fluxes are available from NASA's Goddard Earth Sciences Data and Information Services Center (GES DISC) (Xia, 2014; Xia et al., 2014). MODIS Land Cover Type product (MCD12Q1, Version 6) is available from Google Earth Engine Data Catalog: https://developers.google.com/earth-engine/datasets/catalog/MODIS_061_MCD12Q1 (Friedl et al., 2010). All analyses are performed using Python (Python v3.11, 2024) and MATLAB R2023b (The MathWorks Inc., 2022).

Acknowledgments

This study is supported by the National Science Foundation award numbers 2422542 and 2445027. The authors gratefully acknowledge the Texas A&M University Supercomputing Facility (HPRC) for providing the computational resources that enabled high-resolution spatial analysis.

References

Barton, E. J., Klein, C., Taylor, C. M., Marsham, J., Parker, D. J., Maybee, B., et al. (2025). Soil moisture gradients strengthen mesoscale convective systems by increasing wind shear. *Nature Geoscience*, *18*(4), 330–336. https://doi.org/10.1038/s41561-025-01666-8

Benson, D. O., & Dirmeyer, P. A. (2021). Characterizing the relationship between temperature and soil moisture extremes and their role in the exacerbation of heat waves over the contiguous United States. *Journal of Climate*, *34*(6), 2175–2187. https://doi.org/10.1175/JCLI-D-20-0440.1

Benson, D. O., & Dirmeyer, P. A. (2023). The soil moisture–surface flux relationship as a factor for extreme heat predictability in subseasonal to seasonal forecasts. *Journal of Climate*, *36*(18), 6375–6392. https://doi.org/10.1175/JCLI-D-22-0447.1

Cammalleri, C., McCormick, N., Spinoni, J., & Nielsen-Gammon, J. W. (2024). An analysis of the lagged relationship between anomalies of precipitation and soil moisture and its potential role in agricultural drought early warning. *Journal of Applied Meteorology and Climatology*, *63*(2), 339–350. https://doi.org/10.1175/JAMC-D-23-0077.1

Di Lorenzo, E., & Mantua, N. (2016). Multi-year persistence of the 2014/15 North Pacific marine heatwave. *Nature Climate Change*, *6*(11), 1042–1047. https://doi.org/10.1038/nclimate3082

Dirmeyer, P. A., Balsamo, G., Blyth, E. M., Morrison, R., & Cooper, H. M. (2021). Land-Atmosphere interactions exacerbated the drought and heatwave over Northern Europe during summer 2018. *AGU Advances*, *2*, e2020AV000283. https://doi.org/10.1029/2020AV000283

Donges, J. F., Schleussner, C.-F., Siegmund, J. F., & Donner, R. V. (2016). Event coincidence analysis for quantifying statistical interrelationships between event time series. *The European Physical Journal - Special Topics*, *225*(3), 471–487. https://doi.org/10.1140/epjst/e2015-50233-y

Feng, S., Hao, Z., Zhang, X., & Hao, F. (2019). Probabilistic evaluation of the impact of compound dry-hot events on global maize yields. *The Science of the Total Environment*, *689*, 1228–1234. https://doi.org/10.1016/j.scitotenv.2019.06.373

Ford, T. W., & Labosier, C. F. (2017). Meteorological conditions associated with the onset of flash drought in the Eastern United States. *Agricultural and Forest Meteorology*, *247*, 414–423. https://doi.org/10.1016/j.agrformet.2017.08.031

Ford, T. W., McRoberts, D. B., Quiring, S. M., & Hall, R. E. (2015). On the utility of in situ soil moisture observations for flash drought early warning in Oklahoma, USA. *Geophysical Research Letters*, *42*(22), 9790–9798. https://doi.org/10.1002/2015GL066600

Friedl, M. A., Sulla-Menashe, D., Tan, B., Schneider, A., Ramankutty, N., Sibley, A., & Huang, X. (2010). MODIS Collection 5 global land cover: Algorithm refinements and characterization of new datasets. *Remote Sensing of Environment*, *114*(1), 168–182. https://doi.org/10.1016/j.rse.2009.08.016

Fu, Z., Ciais, P., Wigneron, J.-P., Gentine, P., Feldman, A. F., Makowski, D., et al. (2024). Global critical soil moisture thresholds of plant water stress. *Nature Communications*, *15*(1), 4826. https://doi.org/10.1038/s41467-024-49244-7

Gevaert, A. I., Miralles, D. G., de Jeu, R. a. M., Schellekens, J., & Dolman, A. J. (2018). Soil moisture-temperature coupling in a set of land surface models. *Journal of Geophysical Research: Atmospheres*, *123*(3), 1481–1498. https://doi.org/10.1002/2017JD027346

Ghanbari, M., Arabi, M., Georgescu, M., & Broadbent, A. M. (2023). The role of climate change and urban development on compound dry-hot extremes across US cities. *Nature Communications*, *14*(1), 3509. https://doi.org/10.1038/s41467-023-39205-x

Goodrich, G. B., Thompson, J. K., Wingard, S. D., & Batson, K. J. (2011). The 2007 mid-south summer drought and heat wave in historical perspective. Southeast. *Geogr*, *51*(3), 411–421. https://doi.org/10.1353/sgo.2011.0031

Green, J. K., Konings, A. G., Alemohammad, S. H., Berry, J., Entekhabi, D., Kolassa, J., et al. (2017). Regionally strong feedbacks between the atmosphere and terrestrial biosphere. *Nature Geoscience*, *10*(6), 410–414. https://doi.org/10.1038/ngeo2957

Guo, Z., Dirmeyer, P. A., Koster, R. D., Sud, Y. C., Bonan, G., Oleson, K. W., et al. (2006). GLACE: The global land–atmosphere coupling experiment. Part II: Analysis. *Journal of Hydrometeorology*, *7*(4), 611–625. https://doi.org/10.1175/JHM511.1

Hao, Y., Yuan, X., & Zhang, M. (2024). Enhanced relationship between seasonal soil moisture droughts and vegetation under climate change over China. *Agricultural and Forest Meteorology*, *358*, 110258. https://doi.org/10.1016/j.agrformet.2024.110258

He, X., & Sheffield, J. (2020). Lagged compound occurrence of droughts and pluvials globally over the past seven decades. *Geophysical Research Letters*, *47*(14), e2020GL087924. https://doi.org/10.1029/2020GL087924

Hirschi, M., Mueller, B., Dorigo, W., & Seneviratne, S. I. (2014). Using remotely sensed soil moisture for land–atmosphere coupling diagnostics: The role of surface vs. root-zone soil moisture variability. *Remote Sensing of Environment*, *154*, 246–252. https://doi.org/10.1016/j.rse.2014.08.030

Hirschi, M., Seneviratne, S. I., Alexandrov, V., Boberg, F., Boroneant, C., Christensen, O. B., et al. (2011). Observational evidence for soil-moisture impact on hot extremes in southeastern Europe. *Nature Geoscience*, *4*(1), 17–21. https://doi.org/10.1038/ngeo1032

Ji, Y., Li, Y., Yao, N., Biswas, A., Zou, Y., Meng, Q., & Liu, F. (2021). The lagged effect and impact of soil moisture drought on terrestrial ecosystem water use efficiency. *Ecological Indicators*, *133*, 108349. https://doi.org/10.1016/j.ecolind.2021.108349

Jiang, Y., & Wang, G. (2024). Soil moisture dominates the land surface feedback in the development of compound drought–heat extremes in tropical South America. *Journal of Hydrometeorology*, *25*(11), 1649–1664. https://doi.org/10.1175/JHM-D-24-0005.1

Jiang, Y., Yang, M., Liu, W., Mohammadi, K., & Wang, G. (2022). Eco-hydrological responses to recent droughts in tropical South America. *Environmental Research Letters*, *17*(2), 024037. https://doi.org/10.1088/1748-9326/ac507a

Koster, R. D., Dirmeyer, P. A., Guo, Z., Bonan, G., Chan, E., Cox, P., et al. (2004). Regions of strong coupling between soil moisture and precipitation. *Science*, *305*(5687), 1138–1140. https://doi.org/10.1126/science.1100217

Lemus-Canovas, M., Insua-Costa, D., Trigo, R. M., & Miralles, D. G. (2024). Record-shattering 2023 Spring heatwave in western Mediterranean amplified by long-term drought. *npj Climate and Atmospheric Science*, *7*(1), 25. https://doi.org/10.1038/s41612-024-00569-6

Li, R., Zhang, S., Li, F., Lin, X., Luo, M., Wang, S., et al. (2024). Impact of time-lagging and time-preceding environmental variables on top layer soil moisture in semiarid grasslands. *The Science of the Total Environment*, *912*, 169406. https://doi.org/10.1016/j.scitotenv.2023.169406

Liu, X., He, B., Guo, L., Huang, L., & Chen, D. (2020). Similarities and Differences in the Mechanisms causing the European Summer Heatwaves in 2003, 2010, and 2018. *Earth's Future*, *8*(4), e2019EF001386. https://doi.org/10.1029/2019EF001386

Lo, M.-H., Wu, W.-Y., Tang, L. I., Ryu, D., Rashid, M., & Wu, R.-J. (2021). Temporal changes in land surface coupling strength: An example in a semi-arid Region of Australia. *Journal of Climate*, *34*(4), 1503–1513. https://doi.org/10.1175/JCLI-D-20-0250.1

Lorenz, R., Jaeger, E. B., & Seneviratne, S. I. (2010). Persistence of heat waves and its link to soil moisture memory. *Geophysical Research Letters*, *37*(9). https://doi.org/10.1029/2010GL042764

MacAllister, D. J., MacDonald, A. M., Kebede, S., Godfrey, S., & Calow, R. (2020). Comparative performance of rural water supplies during drought. *Nature Communications*, *11*(1), 1099. https://doi.org/10.1038/s41467-020-14839-3

Manoj, J. A., Guntu, R. K., & Agarwal, A. (2022). Spatiotemporal dependence of soil moisture and precipitation over India. *Journal of Hydrology*, *610*, 127898. https://doi.org/10.1016/j.jhydrol.2022.127898

Maraun, D., Schiemann, R., Ossó, A., & Jury, M. (2025). Changes in event soil moisture-temperature coupling can intensify very extreme heat beyond expectations. *Nature Communications*, *16*(1), 734. https://doi.org/10.1038/s41467-025-56109-0

McColl, K. A., Wang, W., Peng, B., Akbar, R., Short Gianotti, D. J., Lu, H., et al. (2017). Global characterization of surface soil moisture drydowns. *Geophysical Research Letters*, *44*(8), 3682–3690. https://doi.org/10.1002/2017GL072819

Mesinger, F., DiMego, G., Kalnay, E., Mitchell, K., Shafran, P. C., Ebisuzaki, W., et al. (2006). North American regional reanalysis. *Bulletin of the American Meteorological Society*, *87*(3), 343–360. https://doi.org/10.1175/BAMS-87-3-343

Miralles, D. G., Gentine, P., Seneviratne, S. I., & Teuling, A. J. (2019). Land–atmospheric feedbacks during droughts and heatwaves: State of the science and current challenges. *Annals of the New York Academy of Sciences*, *1436*(1), 19–35. https://doi.org/10.1111/nyas.13912

Miralles, D. G., Teuling, A. J., van Heerwaarden, C. C., & Vilà-Guerau de Arellano, J. (2014). Mega-heatwave temperatures due to combined soil desiccation and atmospheric heat accumulation. *Nature Geoscience*, *7*(5), 345–349. https://doi.org/10.1038/ngeo2141

Miralles, D. G., van den Berg, M. J., Teuling, A. J., & de Jeu, R. a. M. (2012). Soil moisture-temperature coupling: A multiscale observational analysis. *Geophysical Research Letters*, *39*(21). https://doi.org/10.1029/2012GL053703

Mishra, A. K., Ines, A. V. M., Das, N. N., Prakash Khedun, C., Singh, V. P., Sivakumar, B., & Hansen, J. W. (2015). Anatomy of a local-scale drought: Application of assimilated remote sensing products, crop model, and statistical methods to an agricultural drought study. *J. Hydrol., Drought processes, modeling, and mitigation*, *526*, 15–29. https://doi.org/10.1016/j.jhydrol.2014.10.038

Mishra, A. K., & Singh, V. P. (2010). A review of drought concepts. *Journal of Hydrology*, *391*(1–2), 202–216. https://doi.org/10.1016/j.jhydrol.2010.07.012

Mitchell, D., Heaviside, C., Vardoulakis, S., Huntingford, C., Masato, G., Guillod, B. P., et al. (2016). Attributing human mortality during extreme heat waves to anthropogenic climate change. *Environmental Research Letters*, *11*(7), 074006. https://doi.org/10.1088/1748-9326/11/7/074006

Mondal, S. K., An, S.-I., Min, S.-K., Jiang, T., & Su, B. (2024). Enhanced soil moisture–temperature coupling could exacerbate drought under net-negative emissions. *npj Climate and Atmospheric Science*, *7*, 1–12. https://doi.org/10.1038/s41612-024-00820-0

Mora, C., Spirandelli, D., Franklin, E. C., Lynham, J., Kantar, M. B., Miles, W., et al. (2018). Broad threat to humanity from cumulative climate hazards intensified by greenhouse gas emissions. *Nature Climate Change*, *8*(12), 1062–1071. https://doi.org/10.1038/s41558-018-0315-6

Mueller, B., & Seneviratne, S. I. (2012). Hot days induced by precipitation deficits at the global scale. *Proceedings of the National Academy of Sciences*, *109*(31), 12398–12403. https://doi.org/10.1073/pnas.1204330109

Mukherjee, S., & Mishra, A. K. (2021). Increase in compound drought and heatwaves in a warming world. *Geophysical Research Letters*, *48*(1), e2020GL090617. https://doi.org/10.1029/2020GL090617

Mukherjee, S., Mishra, A. K., Zscheischler, J., & Entekhabi, D. (2023). Interaction between dry and hot extremes at a global scale using a cascade modeling framework. *Nature Communications*, *14*(1), 277. https://doi.org/10.1038/s41467-022-35748-7

Orth, R., & Seneviratne, S. I. (2012). Analysis of soil moisture memory from observations in Europe. *Journal of Geophysical Research*, *117*(D15). https://doi.org/10.1029/2011JD017366

Orth, R., & Seneviratne, S. I. (2013). Predictability of soil moisture and streamflow on subseasonal timescales: A case study. *Journal of Geophysical Research: Atmospheres*, *118*(19), 10963–10979. https://doi.org/10.1002/jgrd.50846

Python v3.11. (2024). Python software foundation [Software]. *Python Language Reference, version 3.11*. Retrieved from http://www.python.org

Rahmati, M., Amelung, W., Brogi, C., Dari, J., Flammini, A., Bogena, H., et al. (2024). Soil moisture memory: State-of-the-art and the way forward. *Reviews of Geophysics*, *62*(2), e2023RG000828. https://doi.org/10.1029/2023RG000828

Rempe, D. M., & Dietrich, W. E. (2018). Direct observations of rock moisture, a hidden component of the hydrologic cycle. *Proceedings of the National Academy of Sciences*, *115*(11), 2664–2669. https://doi.org/10.1073/pnas.1800141115

Ruscica, R. C., Sörensson, A. A., & Menéndez, C. G. (2014). Hydrological links in Southeastern South America: Soil moisture memory and coupling within a hot spot. *International Journal of Climatology*, *34*, 3641–3653. https://doi.org/10.1002/joc.3930

Schumacher, D. L., Keune, J., Dirmeyer, P., & Miralles, D. G. (2022). Drought self-propagation in drylands due to land–atmosphere feedbacks. *Nature Geoscience*, *15*(4), 262–268. https://doi.org/10.1038/s41561-022-00912-7

Schwitalla, T., Jach, L., Wulfmeyer, V., & Warrach-Sagi, K. (2025). Soil moisture–atmosphere coupling strength over central Europe in the recent warming climate. *Natural Hazards and Earth System Sciences*, *25*(4), 1405–1424. https://doi.org/10.5194/nhess-25-1405-2025

Seager, R., Tzanova, A., & Nakamura, J. (2009). Drought in the Southeastern United States: Causes, variability over the last millennium, and the potential for future hydroclimate change. *Journal of Climate*, *22*(19), 5021–5045. https://doi.org/10.1175/2009JCLI2683.1

Seneviratne, S. I., Corti, T., Davin, E. L., Hirschi, M., Jaeger, E. B., Lehner, I., et al. (2010). Investigating soil moisture–climate interactions in a changing climate: A review. *Earth-Science Reviews*, *99*(3–4), 125–161. https://doi.org/10.1016/j.earscirev.2010.02.004

Seneviratne, S. I., Lüthi, D., Litschi, M., & Schär, C. (2006). Land–atmosphere coupling and climate change in Europe. *Nature*, *443*(7108), 205–209. https://doi.org/10.1038/nature05095

Stéfanon, M., Drobinski, P., D'Andrea, F., Lebeaupin-Brossier, C., & Bastin, S. (2014). Soil moisture-temperature feedbacks at meso-scale during summer heat waves over Western Europe. *Climate Dynamics*, *42*(5–6), 1309–1324. https://doi.org/10.1007/s00382-013-1794-9

Sun, A. Y., Xia, Y., Caldwell, T. G., & Hao, Z. (2018). Patterns of precipitation and soil moisture extremes in Texas, US: A complex network analysis. *Advances in Water Resources*, *112*, 203–213. https://doi.org/10.1016/j.advwatres.2017.12.019

Teuling, A. J., Van Loon, A. F., Seneviratne, S. I., Lehner, I., Aubinet, M., Heinesch, B., et al. (2013). Evapotranspiration amplifies European summer drought. *Geophysical Research Letters*, *40*(10), 2071–2075. https://doi.org/10.1002/grl.50495

The MathWorks Inc. (2022). Matlab 2023 [Software]. Retrieved from https://www.mathworks.com

Tijdeman, E., & Menzel, L. (2021). The development and persistence of soil moisture stress during drought across southwestern Germany. *Hydrology and Earth System Sciences*, *25*(4), 2009–2025. https://doi.org/10.5194/hess-25-2009-2021

Tripathy, K. P., & Mishra, A. K. (2023). How unusual is the 2022 European compound drought and heatwave event? *Geophysical Research Letters*, *50*(15), e2023GL105453. https://doi.org/10.1029/2023GL105453

Tuttle, S. E., & Salvucci, G. D. (2017). Confounding factors in determining causal soil moisture-precipitation feedback. *Water Resources Research*, *53*(7), 5531–5544. https://doi.org/10.1002/2016WR019869

Vasconcelos, V., & Sacht, H. (2020). Influence of canopy cover on surface temperature. *Rev. Bras. Geogr. Física*, *13*(7), 3275–3286. https://doi.org/10.26848/rbgf.v13.07.p3275-3286

Wang, M., Huang, Y., Franzke, C. L. E., Yuan, N., Fu, Z., & Boers, N. (2025). Evidence for preferred propagating terrestrial heatwave pathways due to Rossby wave activity. *Nature Communications*, *16*(1), 4742. https://doi.org/10.1038/s41467-025-60104-w

Williams, A. P., Cook, B. I., & Smerdon, J. E. (2022). Rapid intensification of the emerging southwestern North American megadrought in 2020–2021. *Nature Climate Change*, *12*(3), 232–234. https://doi.org/10.1038/s41558-022-01290-z

Xia, Y., Ek, M., Sheffield, J., Livneh, B., Huang, M., Wei, H., et al. (2013). Validation of Noah-Simulated soil temperature in the north American land data assimilation system phase 2. *Journal of Applied Meteorology and Climatology*, *52*, 455–471. https://doi.org/10.1175/JAMC-D-12-033.1

Xia, Y., Ek, M. B., Wu, Y., Ford, T., & Quiring, S. M. (2015). Comparison of NLDAS-2 simulated and NASMD observed daily soil moisture. Part I: Comparison and analysis. *Journal of Hydrometeorology*, *16*(5), 1962–1980. https://doi.org/10.1175/JHM-D-14-0096.1

Xia, Y., et al. (2014). NLDAS project, NLDAS Noah Land Surface Model L4 Hourly 0.125 x 0.125 degree V2.0 [Dataset], *NASA/GSFC/HSL, Greenbelt, Maryland, USA, Goddard Earth sciences data and information services Center (GES DISC)*. In D. Mocko (Ed.). https://doi.org/10.5067/T4OW83T8EXDO

Xia, Y., Mitchell, K., Ek, M., Sheffield, J., Cosgrove, B., Wood, E., et al. (2012). Continental-scale water and energy flux analysis and validation for the North American Land Data Assimilation System project phase 2 (NLDAS-2): 1. Intercomparison and application of model products. *Journal of Geophysical Research*, *117*(D3). https://doi.org/10.1029/2011JD016048

Xia, Y., Sheffield, J., Ek, M. B., Dong, J., Chaney, N., Wei, H., et al. (2014). Evaluation of multi-model simulated soil moisture in NLDAS-2. *Journal of Hydrology*, *512*, 107–125. https://doi.org/10.1016/j.jhydrol.2014.02.027

Zampieri, M., Ceglar, A., Dentener, F., & Toreti, A. (2017). Wheat yield loss attributable to heat waves, drought and water excess at the global, national and subnational scales. *Environmental Research Letters*, *12*(6), 064008. https://doi.org/10.1088/1748-9326/aa723b

Zeng, X. (2001). Global vegetation root distribution for land modeling. *Journal of Hydrometeorology*, *2*(5), 525–530. https://doi.org/10.1175/1525-7541(2001)002<0525:gvrdfl>2.0.co;2

Zhang, B., Xia, Y., Long, B., Hobbins, M., Zhao, X., Hain, C., et al. (2020). Evaluation and comparison of multiple evapotranspiration data models over the contiguous United States: Implications for the next phase of NLDAS (NLDAS-Testbed) development. *Agricultural and Forest Meteorology*, *280*, 107810. https://doi.org/10.1016/j.agrformet.2019.107810

Zhou, S., Williams, A. P., Berg, A. M., Cook, B. I., Zhang, Y., Hagemann, S., et al. (2019). Land–atmosphere feedbacks exacerbate concurrent soil drought and atmospheric aridity. *Proceedings of the National Academy of Sciences*, *116*(38), 18848–18853. https://doi.org/10.1073/pnas.1904955116

References From the Supporting Information

Alessi, M. J., Herrera, D. A., Evans, C. P., DeGaetano, A. T., & Ault, T. R. (2022). Soil moisture conditions determine land-atmosphere coupling and drought risk in the Northeastern United States. *Journal of Geophysical Research: Atmospheres*, *127*(6), e2021JD034740. https://doi.org/10.1029/2021JD034740

Dirmeyer, P. A., Schlosser, C. A., & Brubaker, K. L. (2009). Precipitation, recycling, and land memory: An integrated analysis. *Journal of Hydrometeorology*, *10*(1), 278–288. https://doi.org/10.1175/2008JHM1016.1

Ekström, M., Jones, P. D., Fowler, H. J., Lenderink, G., Buishand, T. A., & Conway, D. (2007). Regional climate model data used within the SWURVE project – 1: Projected changes in seasonal patterns and estimation of PET. *Hydrology and Earth System Sciences*, *11*(3), 1069–1083. https://doi.org/10.5194/hess-11-1069-2007

Koster, R. D., & Suarez, M. J. (2001). Soil moisture memory in climate models. *Journal of Hydrometeorology*, *2*(6), 558–570. https://doi.org/10.1175/1525-7541(2001)002<0558:SMMICM>2.0.CO;2

Mitchell, K. E., Lohmann, D., Houser, P. R., Wood, E. F., Schaake, J. C., Robock, A., et al. (2004). The multi-institution North American Land Data Assimilation System (NLDAS): Utilizing multiple GCIP products and partners in a continental distributed hydrological modeling system. *Journal of Geophysical Research*, *109*(D7). https://doi.org/10.1029/2003JD003823

Niu, G.-Y., Yang, Z.-L., Mitchell, K. E., Chen, F., Ek, M. B., Barlage, M., et al. (2011). The community Noah land surface model with multiparameterization options (Noah-MP): 1. Model description and evaluation with local-scale measurements. *Journal of Geophysical Research*, *116*(D12), D12109. https://doi.org/10.1029/2010JD015139

Vicente-Serrano, S. M., Beguería, S., & López-Moreno, J. I. (2010). A multiscalar drought index sensitive to global warming: The standardized precipitation evapotranspiration index. *Journal of Climate*, *23*(7), 1696–1718. https://doi.org/10.1175/2009JCLI2909.1